Radiative lifetimes of dipolar excitons in double quantum wells

Yotam Mazuz-Harpaz, Kobi Cohen, Boris Laikhtman, and Ronen Rapaport*
Racah Institute of Physics, The Hebrew University of Jerusalem, Jerusalem 9190401, Israel

Ken West and Loren N. Pfeiffer
Department of Electrical Engineering, Princeton University, Princeton, New Jersey 08544, USA
(Received 18 October 2016; revised manuscript received 13 March 2017; published 4 April 2017)

Spatially indirect excitons in semiconducting double quantum wells have been shown to exhibit rich collective many-body behavior that results from the nature of the extended dipole-dipole interactions between particles. For many spectroscopic studies of the emission from a system of such indirect excitons, it is crucial to separate the single-particle properties of the excitons from the many-body effects arising from their mutual interactions. In particular, knowledge of the relation between the emission energy of indirect excitons and their radiative lifetime could be highly beneficial for control, manipulation, and analysis of such systems. Here we study a simple analytic approximate relation between the radiative lifetime of indirect excitons and their emission energy. We show, both numerically and experimentally, the validity and the limits of this approximate relation. This relation between the emission energy and the lifetime of indirect excitons can be used to tune and determine their lifetime and their resulting dynamics without the need of directly measuring it, and as a tool for design of indirect exciton based devices.

DOI: 10.1103/PhysRevB.95.155302

I. INTRODUCTION

An indirect exciton (IX) is a Coulomb-bound complex of an electron (e) and a hole (h) where the opposite charges of the bound complex are spatially separated in two parallel layers with a tunneling barrier between them, as is depicted in Fig. 1. Such IXs are usually formed by optical excitation of an electrically biased double quantum well (DQW) heterostructure [1–3]. This spatial $e-h$ separation leads to a long radiative lifetime and to a large electrical dipole moment of the IX. Due to the combination of these two properties, IXs give a unique opportunity to observe and study interesting cold interacting low-dimensional fluids.

In recent years, an intensive experimental and theoretical effort focused on IX fluids in GaAs based DQWs revealed many intriguing phenomena, such as spontaneous pattern formation [4–7], spin textures [8], interaction-induced particle correlations [9,10], molecular IX complexes [11,12], as well as evidence for complex collective phases [10,13–17]. On the other hand, recent progress in the techniques for control and manipulation of IXs led to demonstration of various kinds of complex device functionalities such as trapping schemes [11,18–21], flow control, IX transport and routing [22–26], and spin transport [27,28]. Due to these recent advancements, cold IX fluids started attracting the interest of a wider scientific community, and new experiments on dipolar fluids of IXs in newly emerging systems have been performed recently. These include bilayer two-dimensional transition-metal dichalcogenide systems [29,30], bilayer graphene [31,32], and polaritonic systems [33–36] among others.

To fully understand and control the various properties of such optically generated IX fluids, it is very important to have a good insight on their intrinsic dynamics. A key property of the IX dynamics is the radiative lifetime. This radiative lifetime due to the $e-h$ optical recombination is the dominant loss process in such systems, and can in principle be measured directly by time-resolved measurement of the decay of their photoluminescence after a pulse excitation [37–40]. However, as many experiments are done in a steady state under continuous-wave excitation and do not involve a direct lifetime measurement, a method of inferring the lifetime from other measurable quantities can be very useful. In particular, when designing a sample, a complex device, or an experiment, a prior knowledge and understanding of such recombination dynamics could be essential.

Previous theoretical works have proposed various approaches allowing calculation of the lifetime of IXs [41–52]. These have considered some of the sources for the complexity of the general problem, such as the three-dimensional shape of the wave function of the bound $e-h$ pair, effect of strong IX localization, and other effects. Here we discuss a simpler approach, proposed in our previous work [10], according to which the radiative lifetime of an IX is simply related to its emission energy. This approach disregards many of the aspects addressed by the more general models, limiting its own validity to certain conditions, in order to reach a very simple method to extract lifetimes for IXs. Nevertheless, as we show below, despite its simplicity the model obtained is still expected to be accurate under a wide range of experimentally accessible parameters.

The model of Ref. [10] considers the recombination lifetime of an IX as being inversely proportional to the squared overlap integral between the envelope wave functions of the e and the h along the DQW growth direction z:

$$\tau_{id} = \frac{\tau_d}{|\langle\psi_e|\psi_h\rangle|^2} \tag{1}$$

where τ_{id} and τ_d are the lifetimes of the IX and of the direct exciton (DX), respectively, and ψ_e and ψ_h are the envelope wave functions of the e and the h along the z axis, respectively.

*ronenr@phys.huji.ac.il

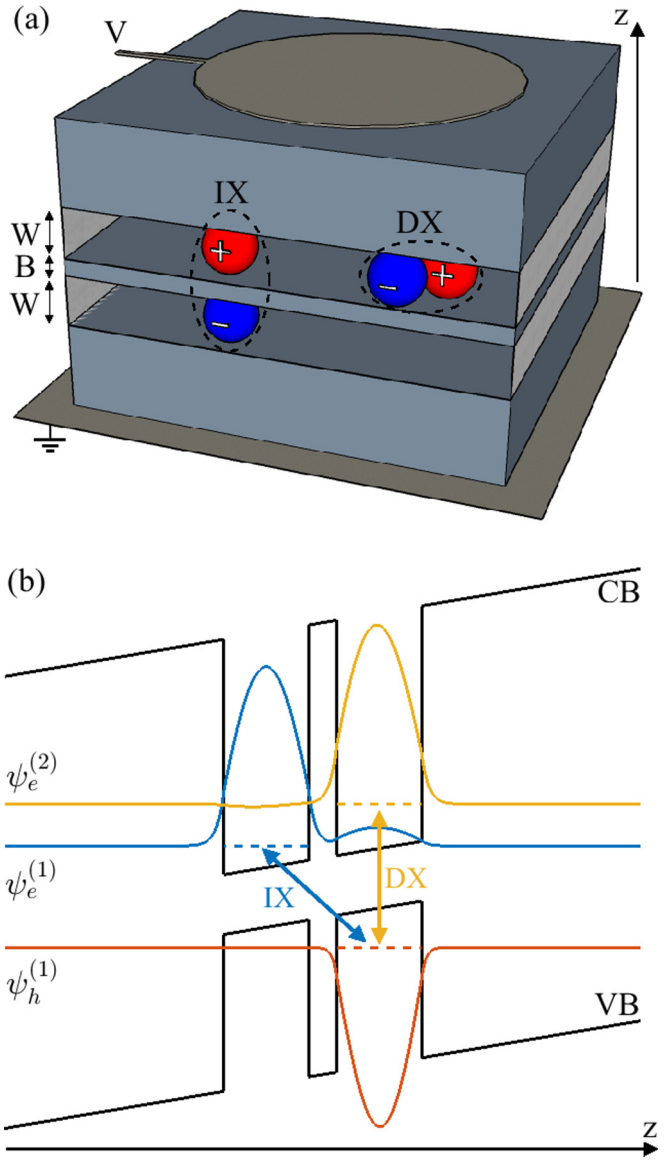

FIG. 1. (a) A simplified illustration of the typical realization of IXs in semiconductor DQW heterostructure. Two quantum wells of width W are separated by a thin central barrier layer marked as B. A metallic gate is positioned on the top of the sample, allowing the induction of the electric field in the z direction. Bound pairs of e (blue sphere) and h (red sphere) are created in the wells by optical excitation and can occupy the DX state, where both particles reside in the same well, or in the IX state, where each of them resides in a different well. (b) A typical energy diagram, illustrating the conduction (CB) and valence (VB) energy bands along the z axis, the wave functions of the h (red line) and the e occupying the DX (yellow line) and IX (blue line) states, and their corresponding energies (dashed lines). The external electric field is responsible for the tilt of the energy bands, making the IX state lower in energy than the DX state.

Figure 1 schematically illustrates both the DX and IX states in a DQW under an applied electric field along the z axis.

Under a weak enough external electric field, the envelope wave functions of the e and the h in their lowest-energy states can be approximated as a linear combination of the corresponding lowest-energy flat-band single quantum well (SQW) wave functions [53]:

$$\psi_e(z) = c_e^l \psi_e^l(z) + c_e^r \psi_e^r(z), \tag{2a}$$

$$\psi_h(z) = c_h^l \psi_h^l(z) + c_h^r \psi_h^r(z). \tag{2b}$$

Initially, increasing the field will only affect the coefficients and not the validity of the approximation itself. However, when the field becomes strong enough such that the potential drop across each QW is of the order of the difference between the ground energy in the SQW and its first excited-state energy, this approximation breaks. Such strong field leads to a substantial admixture of excited states, shifting the peak of each wave function away from the tunneling barrier. Another approximation can be made in cases where the effective mass of the h is significantly larger than the effective mass of the e, and under a large enough external field. In such case, the lowest-energy h's wave function can be well approximated by only one SQW wave function, i.e., $\psi_h(z) = \psi_h^r(z)$ in the case of an electric field applied in the positive z direction, as is illustrated in Fig. 1(b). As a result, if the external field is strong enough, the computation of the overlap integral $\langle\psi_e|\psi_h\rangle$ of Eq. (1) can be approximated by integration of the e's wave function only inside the right QW, where the h's wave function is strongly confined. Thus, there is an intermediate range of electric-field values in which both of the above approximations should hold to a good accuracy. Within this range, the computation of the recombination lifetime is reduced to the computation of c_e^r—the amplitude of the e's wave function in the h's well:

$$\tau_{id} = \frac{\tau_d}{|c_e^r|^2}. \tag{3}$$

As was shown in Ref. [10], the solution of the problem in the basis of ψ_e^l and ψ_e^r yields

$$c_e^r = \frac{1}{\sqrt{2}}\sqrt{1 - \frac{E_d - E_{id}}{\sqrt{(E_d - E_{id})^2 + 4v_e^2}}} \tag{4}$$

where E_d and E_{id} are the energies of the DX and IX, respectively, and v_e is the following tunneling matrix element for the e:

$$v_e = \langle\psi_e^l|(\mathcal{T} + V_e(z))|\psi_e^r\rangle - \langle\psi_e^l|\psi_e^r\rangle E_0. \tag{5}$$

Here, $\mathcal{T}$ is the kinetic energy, $V_e(z)$ is the DQW potential felt by the electron, and E_0 is the ground-state energy of a noninteracting electron in a SQW potential. The expression in Eq. (5) is obtained under the assumption that all other contributions to v_e (i.e., the external electric field, the interaction of the electron with neighboring IXs, and its Coulomb interaction with the h) are negligible. As explained above, Eq. (4) is expected to be valid where the following conditions are satisfied:

$$v_h \ll v_e, \tag{6a}$$

$$v_h \ll E_d - E_{id} \ll E_d^{(1)} - E_d^{(0)} \tag{6b}$$

where v_h is the corresponding tunneling matrix element for the h and $E_d^{(n)}$ is the n'th DX energy level in a flatband SQW. Additionally, in cases where also the following condition is

satisfied,

$$v_e \ll \tfrac{1}{2}(E_d - E_{id}), \tag{7}$$

Eq. (4) is reduced to

$$c_e^r = \frac{v_e}{E_d - E_{id}}. \tag{8}$$

In such case, the radiative lifetime of an IX can approximately be expressed as [10]

$$\frac{1}{\tau_{id}} = \frac{1}{\tau_d}\frac{v_e^2}{(E_d - E_{id})^2}. \tag{9}$$

It is worth mentioning the Coulomb binding between the e and the h within an IX. A three-dimensional treatment of the problem shows that the binding energy of an IX may shift due to variation of the external field and the IX-IX interaction, over a few milli-electron-volts in samples such as that discussed here [48]. This, off course, might have impaired the validity of the discussed model. However, as shown in the Appendix, within the range defined in Eq. (6) this shift is expected to be approximately identical for the DX and the IX, such that its effect on the quantity $E_d - E_{id}$—and thus also on the accuracy of the model within that range—is negligible.

In this paper we numerically test the accuracy and validity limits of Eq. (9) and provide an experimental confirmation of it for a few combinations of experimental parameters which lie within the expected validity range. The structure of this paper is as follows. In Sec. II we compare that analytic result to a numerical calculation using a coupled Schrödinger-Poisson solver under a mean-field approximation of the interactions between IXs. In Sec. III we present experimental results confirming the validity of Eq. (9) and of the underlying approximations. In Sec. IV we summarize our results and their conclusions.

II. COMPARISON TO NUMERICAL CALCULATIONS

To check the validity, accuracy, and applicability limits of Eq. (9), we first compared its predictions with numerical calculations of the overlap between the envelope wave functions of the e and the h, using a one-dimensional, self-consistent, Schrödinger-Poisson solver [54]. In the numerical model, we assumed a mean-field approximation for the IX-IX interactions, where in-plane dipolar correlations [9] were neglected, as well as the binding interaction between the e and the h. For any given applied field F and IX density n, we obtained from the solver the envelope wave functions for the e and for the h and numerically computed their overlap integral. The IX radiative lifetime is inversely proportional to the square of this overlap integral, and thus it can be calculated up to a multiplicative constant. More importantly, the ratio between the lifetime of the DX and the IX can also be calculated in this way as

$$\frac{\tau_{id}}{\tau_d} = \frac{\left|\left\langle\psi_e^{(2)}\middle|\psi_h^{(1)}\right\rangle\right|^2}{\left|\left\langle\psi_e^{(1)}\middle|\psi_h^{(1)}\right\rangle\right|^2} \tag{10}$$

where the superscripts mark the corresponding quantum number of the e and h energy levels in the DQW. Substituting Eq. (3) we get the following equation:

$$\frac{\left|\left\langle\psi_e^{(2)}\middle|\psi_h^{(1)}\right\rangle\right|^2}{\left|\left\langle\psi_e^{(1)}\middle|\psi_h^{(1)}\right\rangle\right|^2} = \frac{1}{\left|c_e^r\right|^2}, \tag{11}$$

the right-hand side of which is determined either by Eq. (4) or by its approximation, Eq. (8). Since the same numerical solver also yields $E_d - E_{id}$, the accuracy of this equality can be used to check the accuracy of Eq. (3), after plugging in the amplitude c_e^r and the e's tunneling matrix element v_e.

TABLE I. The tunneling matrix element values, for the e and for the hh, in the four DQW structures discussed in Sec. II: $Al_{0.5}Ga_{0.5}As/GaAs/Al_{0.5}Ga_{0.5}As$ of layer width $W/4\text{nm}/W$.

W (nm)	v_e (meV)	v_h (meV)
8	0.33	0.003
10	0.2	0.002
12	0.12	0.001
14	0.08	0.0007

The tunneling matrix element v_e can be calculated numerically using the SQW wave functions ψ_e^r and ψ_e^l according to Eq. (5) and the h's tunneling matrix element v_h can be calculated similarly. We carried this calculation for the heavy-hole IX in four different realistic GaAs DQW structures: $Al_{0.5}Ga_{0.5}As/GaAs/Al_{0.5}Ga_{0.5}As$ of layer width $W/4$ nm$/W$ differing by their well width W. Their resulted values are presented in Table I.

The relative error Δ of Eq. (11) is defined as (r.h.s-l.h.s)/l.h.s, i.e.,

$$\Delta \equiv \frac{1}{\left|c_e^r\right|^2} \times \frac{\left|\left\langle\psi_e^{(1)}\middle|\psi_h^{(1)}\right\rangle\right|^2}{\left|\left\langle\psi_e^{(2)}\middle|\psi_h^{(1)}\right\rangle\right|^2} - 1. \tag{12}$$

This error was computed and is presented in Fig. 2(a) as a function of $E_d - E_{id}$ for the aforementioned four different DQW structures for the single-IX case (i.e., where the IX-IX interaction is set to zero). It is computed both using c_e^r as defined in Eq. (4) (continuous curves) and its first-order approximation, Eq. (8) (dashed). The dependence of the relative error Δ on $E_d - E_{id}$ is in agreement with the expected limits of validity mentioned in the previous section, where $E_d - E_{id}$ is very small, the penetration of the h's wave function into the e's QW is significant, and using Eq. (4) we get an overestimation of the radiative lifetime. Once the field is increased such that $E_d - E_{id}$ becomes much larger than v_e, the error drops rapidly and stays low for quite a wide range of $E_d - E_{id}$ values. At even larger values of $E_d - E_{id}$, both the e's and the h's wave functions distort in opposite directions and their overlap integral is further diminished. The analytic model does not take this distortion into account (as each of the basis wave functions used ψ^l and ψ^r is of a flat bottom QW), and so it underestimates the lifetime, resulting in a relative error which grows with $E_d - E_{id}$ in the negative direction. As expected, this distortion increases with the width of the QWs, leading to a wider $E_d - E_{id}$ range having a high relative accuracy of Eq. (9) for narrower DQWs. Interestingly, the algebraic approximation leading from Eq. (4) to Eq. (8) contributes an error which in low energies is opposite in its

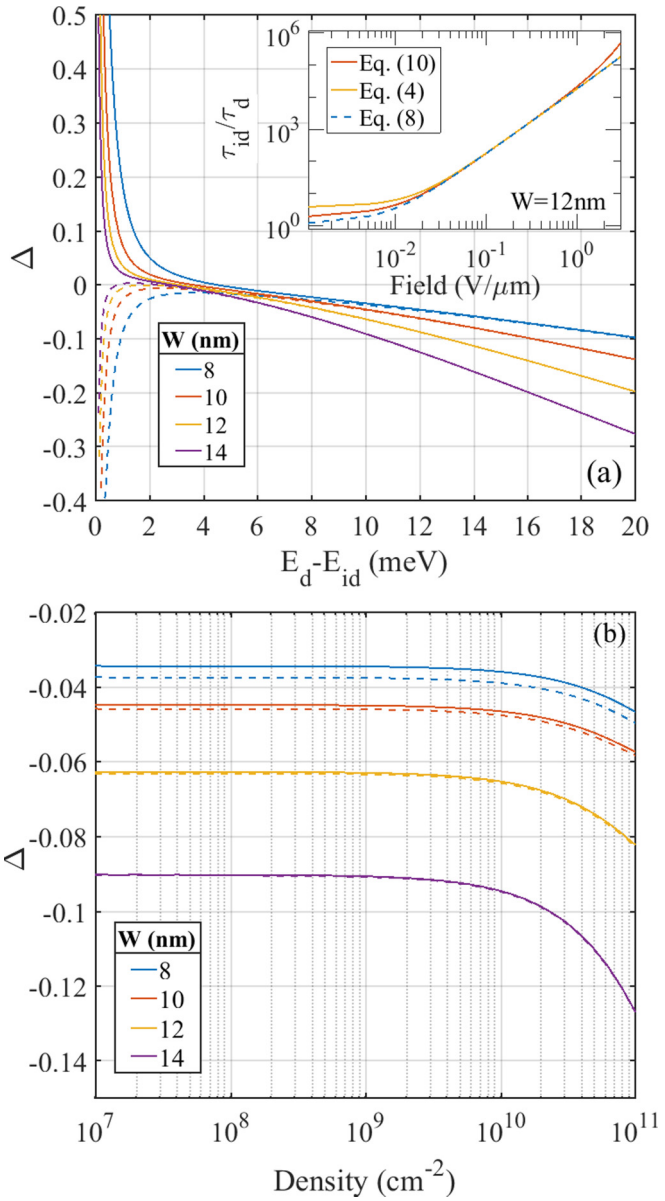

FIG. 2. (a) The relative error Δ of Eq. (11), defined in Eq. (12), plotted against $E_d - E_{id}$ for four different well widths (W) of a $Al_{0.5}Ga_{0.5}As/GaAs/Al_{0.5}Ga_{0.5}As$ DQW structure having tunneling barrier of width $B = 4$ nm. It is computed both using Eq. (4) (continuous lines) and using Eq. (8) (dashed lines). The inset demonstrates the source of the calculated values of Δ for the structure where $W = 12$ nm, by showing the calculated IX lifetime vs the external field. The red curve represents the results obtained numerically, according to Eq. (10); the yellow curve represents the lifetimes predicted according to Eq. (8); and the dashed blue curve represents the lifetimes predicted according to the further approximated Eq. (8). (b) Δ as a function of the IX density n while the external field is adjusted to keep the constant value of $E_d - E_{id} = 10$ meV, for each of the four DQW structures.

sign to the fundamental errors of Eq. (4), as demonstrated in the inset of Fig. 2(a). Thus, at low energies the errors tend to cancel each other, making the prediction based on Eq. (8) accurate in a wider range of energies.

Figure 2(b) presents the relative error as a function of the IX density n, for a fixed value $E_d - E_{id} = 10$ meV. This is done by setting different values of n and finding the corresponding values of F to keep $E_d - E_{id}$ constant (this method, named the "constant energy line method," was extensively used in our previous experimental works [10,17]). As seen in the figure, the relatively low error values are maintained up to a high IX density of $n \simeq 10^{11}$ cm^{-2}. This demonstrates the robustness of the model also in a multiparticle problem, where the IX-IX interaction may effect E_{id} significantly. Above this density value, the inhomogeneous distribution of the IX charge density along the z axis of the QWs is large enough to induce large deviations of the e and h wave functions from the single-particle wave functions, leading to a decrease in the accuracy of the model. In the mean-field approximation used here, this can roughly be formulated, using the plate-capacitor formula [9], as the following additional limitation on the validity of the model:

$$\frac{4\pi e^2 dn}{\kappa} \ll E_d^{(1)} - E_d^{(0)} \tag{13}$$

where e is the elementary charge, d is the separation between the centers of the wells, and κ is the dielectric constant.

These numerical calculations indicate that Eq. (9) is a good approximation over a significant range of applied electric fields and IX densities and can be tested in experiments, as we show in the next section.

III. COMPARISON TO EXPERIMENTS

A. Experimental details

The experimental scheme is rather similar to that presented in a few of our previous works [10,17]. The sample, positioned in an optical ^{4}He cryostat, is a 12/4/12-nm $Al_{0.5}Ga_{0.5}As/GaAs/Al_{0.5}Ga_{0.5}As$ DQW structure grown on an n^+-doped GaAs substrate and with a 10-nm-thick, semitransparent Ti electrode positioned on its top [17]. The overall thickness of the intrinsic part of the sample is about 1.5 μm. An electric field between the top electrode and the doped substrate creates the energy-band tilt required for the formation of IXs and allows their trapping as presented in Figs. 3(a) and 3(b). The sample temperature is maintained at $T = 1.8$ K (± 0.1 K).

A population of IXs is being excited using a nonresonant pulsed laser having a wavelength of 775 nm and a pulse duration of 300 ps, under a fixed applied electric bias. We then study the decay of the population after the pulse excitation, by time-resolved measurement of the light emitted by recombination of the optically active (i.e., "bright") IXs, using a fast-gated intensified CCD camera (Princeton Instruments PIMAX).

B. Results

Exemplary time-resolved spatially integrated spectra at different times after the laser excitation are presented in Fig. 3(c), for a fixed applied bias of 1 V. The spectral lines have a tail to the long-wavelength side, similar to previous results. Figures 3(d) and 3(e) presents the integrated intensity and the IX energy as a function of time after the excitation. The

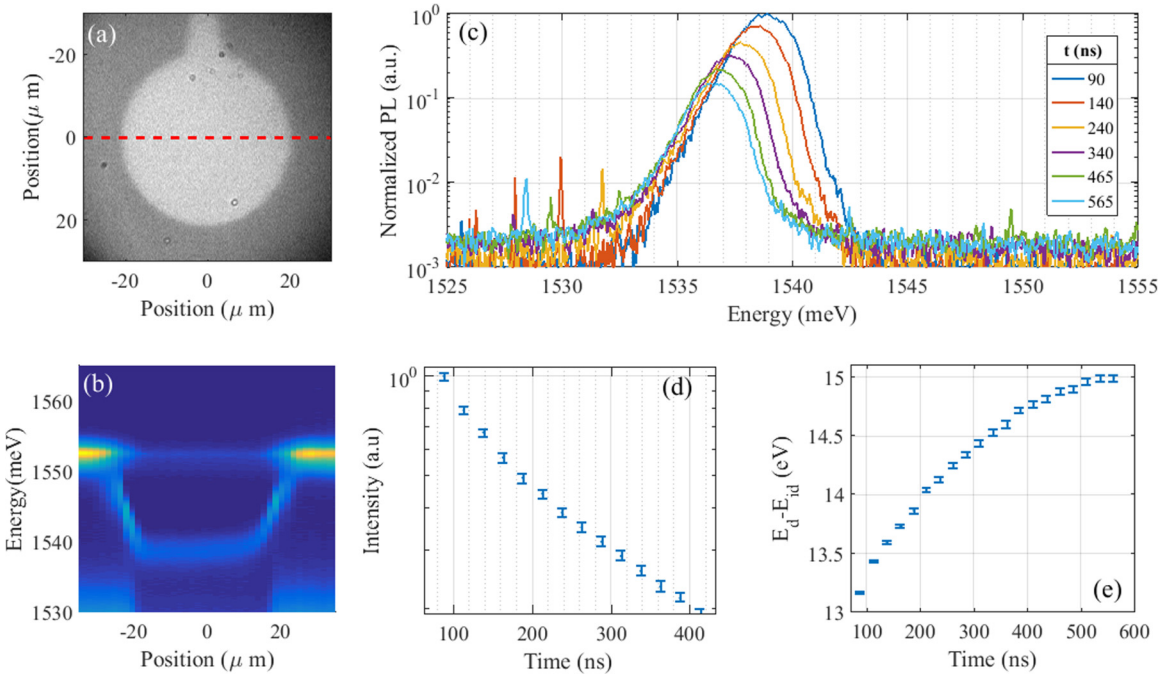

FIG. 3. (a) A real-space image of the circular electrostatic trap used in this paper. (b) A spectral-spatial image of the emission from the sample as a function of the position of a CW laser excitation along the dashed red line drawn in (a), with a reversed voltage set to 1 V, an excitation pulse power of 25 mW and temperature of 1.8 K. The trapping potential is flat around the center of the trap with $E_d - E_{id} \simeq 12$ meV. (c) Exemplary time-resolved and spatially integrated spectra at different times after the laser excitation. (d) Integrated intensity I and (e) $E_d - E_{id}$ as a function of time after the laser pulse extracted from the data in (c). All time frames are integrated over a 25-ns-wide window.

observed redshift during the decay results from the decrease of the interaction energy as the IX density decreases [10].

The radiative recombination of IXs can be described by a simple rate equation:

$$I(t) \propto \frac{\partial n}{\partial t} = \frac{n(t)}{\tau_{id}(t)} \tag{14}$$

where I is the measured emission intensity and τ_{id} is generally time dependent. Using $n(t) \propto \int_t^\infty I(t')dt'$ and expressing $\tau_{id}(t)$ using Eq. (9) the following relation is obtained:

$$I(t) \propto \frac{\int_t^\infty I(t')dt'}{(E_d - E_{id}(t))^2} \equiv G(t) \tag{15}$$

and both $I(t)$ and $G(t)$ can be directly expressed for every t from the experimental results in Figs. 3(d) and 3(e). The assumptions made in this last derivation are the accuracy of Eq. (9) and that the recombination process is radiatively dominated. Thus, if these assumptions are valid we expect that Eq. (15) should hold for our experimental results, i.e., we expect to find that $G(t) \propto I(t)$ for every t along the whole decay. This is therefore a direct experimental test for Eq. (9).

Figure 4 presents the experimentally extracted $G(t)$ versus $I(t)$ for four different decay traces that were measured under different external applied biases and laser powers. The solid lines are linear fits to the data. This figure shows early time dynamics, $t < 300$ ns, where the density is highest such that the changes in τ_{id} and in E_{id} are most significant. A clear linear dependence appears, which is consistent with the above assumptions and is therefore consistent with Eq. (9).

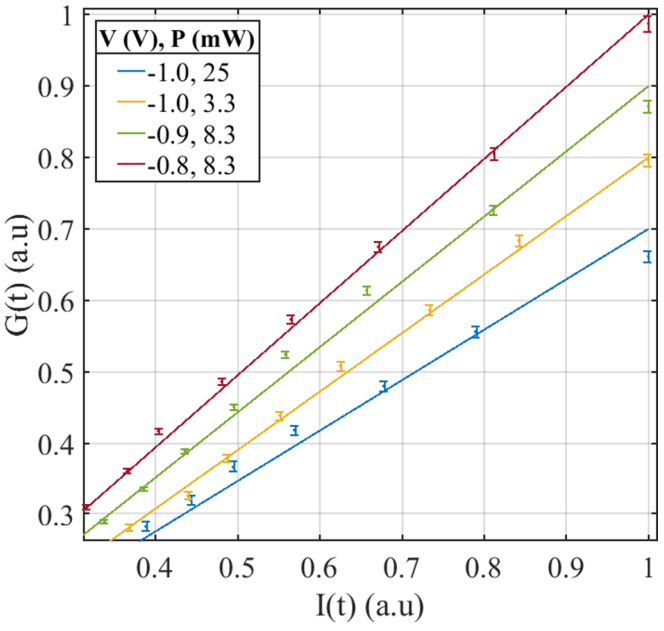

FIG. 4. Experimentally extracted $G(t)$ vs $I(t)$ during $t < 300$ ns for four different decay traces that were measured under fixed lattice temperature of 1.8 K ($\pm$0.1 K) and different combinations of externally applied bias V and laser pulse power P. The solid lines are linear fits to the data. A clear linear dependence is observed, confirming the validity of Eq. (9) for these experimental parameters (the temporal dynamics in each of these measurements is from top right to bottom left).

IV. CONCLUSION

In this paper we presented a numerical and experimental test of an approximated derivation relating the IX radiative lifetime to its energy. We showed that this relation is expected to hold well for a wide range of accessible experimental parameters and thus also supported the assumptions used in our previous works [10,17]. We conclude that this relation can be very useful for future works studying IXs in similar bilayer systems, simplifying the analysis of dynamics of IX systems. In many such experiments, the lifetime is a key property the assessment of which is not a straightforward task under the required experimental settings. This difficulty could be relieved by the proposed method, which in principle requires a single calibration measurement to set right the proportion coefficient of Eq. (9) for the sample of interest.

As demonstrated above by the numerical simulation, Eq. (9) is only expected to be valid and accurate enough in an intermediate range of IX energies: The basic picture described by the theoretical model becomes valid only when the separation between the energies of the indirect and the direct excitons is large enough. As the separation is increased further, the accuracy of the model gradually deteriorates and the error of Eq. (9) grows. Between these two ends lies the range of IX energies where the error is relatively low and Eq. (9) can be used as a good approximation.

We believe that this method can be easily modified for other IX structures that are currently being explored, such as IXs in bilayers of other material systems.

ACKNOWLEDGMENTS

We would like to thank Masha Vladimirova for fruitful discussions. We would also like to acknowledge financial support from the German Deutsche Forschungsgemeinschaft (Grant No. SA-598/9), from the German Israeli Foundation (Grant No. GIF I-1277-303.10/2014), and from the Israeli Science Foundation (Grant No. 1319/12). The work at Princeton University was funded by the Gordon and Betty Moore Foundation through the Emergent Phenomena in Quantum Systems initiative Grant No. GBMF4420, and by the National Science Foundation Materials Research Science and Engineering Center Grant No. DMR-1420541.

APPENDIX: EXCITON BINDING

To take the exciton binding into account for the case that the h's tunneling is negligible, one has to solve the following three-dimensional Schrödinger equation:

$$-\mathcal{T}\phi^r + \left(U^r - \frac{e^2}{\kappa r}\right)\phi^r + \Gamma\phi^l = E\phi^r, \quad \text{(A1a)}$$

$$-\mathcal{T}\phi^l + \left(U^l - \frac{e^2}{\kappa\sqrt{r^2+d^2}}\right)\phi^l + \Gamma\phi^r = E\phi^l \quad \text{(A1b)}$$

where $\phi \equiv (\phi^r,\phi^l)$ is the wave function of the relative position of the e and the h, $\mathcal{T}$ is the kinetic energy, U^r and U^l are the energies above the bottom of each well, $\boldsymbol{r}$ is the in-plane separation between the e and the h, d is the separation between the centers of the wave functions of the e and the h in the z direction, and Γ is the tunneling energy.

The derivation below does not attempt to obtain a solution for these equations, but rather to use them to estimate the accuracy of the model discussed in the main text, considering the $e-h$ Coulomb binding. For that sake, a spectrum of basis in-plane wave functions can be defined by the following Schrödinger equations:

$$-\mathcal{T}\phi_d^{(n)} - \frac{e^2}{\kappa r}\phi_d^{(n)} = -\epsilon_d^{(n)}\phi_d^{(n)}, \quad \text{(A2a)}$$

$$-\mathcal{T}\phi_{id}^{(n)} - \frac{e^2}{\kappa\sqrt{r^2+d^2}}\phi_{id}^{(n)} = -\epsilon_{id}^{(n)}.\phi_{id}^{(n)}. \quad \text{(A2b)}$$

The wave function (ϕ^l,ϕ^r) can thus be expanded:

$$\phi^r(\boldsymbol{r}) = \sum_n c_d^{(n)}\phi_d^{(n)}(\boldsymbol{r}), \quad \text{(A3a)}$$

$$\phi^l(\boldsymbol{r}) = \sum_n c_{id}^{(n)}\phi_{id}^{(n)}(\boldsymbol{r}). \quad \text{(A3b)}$$

Substitution of that expansion in Eqs. (A2), multiplication by $\phi_d^{(n)}$ and by $\phi_{id}^{(n)}$, and integration in plane yields the following equations for the coefficients:

$$\left(U^r + \epsilon_d^{(n)}\right)c_d^{(n)} + \Gamma\sum_{n'}\langle\phi_d^{(n)}|\phi_{id}^{(n')}\rangle c_{id}^{(n')} = Ec_d^{(n)}, \quad \text{(A4a)}$$

$$\left(U^l + \epsilon_{id}^{(n)}\right)c_{id}^{(n)} + \Gamma\sum_{n'}\langle\phi_{id}^{(n)}|\phi_d^{(n')}\rangle c_d^{(n')} = Ec_{id}^{(n)}. \quad \text{(A4b)}$$

Under consideration of the ground exciton states ($n=0$) alone and under the following assumption,

$$\langle\phi_d^{(0)}|\phi_{id}^{(n')}\rangle \approx \langle\phi_d^{(0)}|\phi_{id}^{(0)}\rangle\delta_{n',0}, \quad \text{(A5a)}$$

$$\langle\phi_{id}^{(0)}|\phi_d^{(n')}\rangle \approx \langle\phi_{id}^{(0)}|\phi_d^{(0)}\rangle\delta_{n',0}, \quad \text{(A5b)}$$

Eqs. (A4) are reduced to

$$\left(U^r + \epsilon_d^{(0)}\right)c_d^{(0)} + \Gamma\langle\phi_d^{(0)}|\phi_{id}^{(0)}\rangle c_{id}^{(0)} = Ec_d^{(0)}, \quad \text{(A6a)}$$

$$\left(U^l + \epsilon_{id}^{(0)}\right)c_{id}^{(0)} + \Gamma\langle\phi_d^{(0)}|\phi_{id}^{(0)}\rangle c_d^{(0)} = Ec_{id}^{(0)}. \quad \text{(A6b)}$$

Finally, identifying

$$E_d = U^r + \epsilon_d^{(0)}, \quad E_{id} = U^l + \epsilon_{id}^{(0)} \quad \text{(A7)}$$

and

$$u = \Gamma\langle\phi_d^{(0)}|\phi_{id}^{(0)}\rangle = \Gamma\langle\phi_{id}^{(0)}|\phi_d^{(0)}\rangle, \quad \text{(A8)}$$

it is straightforward to show that Eqs. (A6) also lead to the relation of Eq. (4). Thus, even with the exciton binding taken into account, the model and its result of Eq. (9) are valid, limited by the following condition:

$$\left|\langle\phi_{id}^{(n)}|\phi_d^{(0)}\rangle\right| \ll \left|\langle\phi_{id}^{(0)}|\phi_d^{(0)}\rangle\right|, \quad \text{(A9a)}$$

$$\left|\langle\phi_{id}^{(0)}|\phi_d^{(n)}\rangle\right| \ll \left|\langle\phi_{id}^{(0)}|\phi_d^{(0)}\rangle\right| \quad \text{(A9b)}$$

for every $n>0$. This condition is roughly the same condition as the right-hand side of Eq. (6b), which implies that as a matter of fact the model discussed in the main text already accounts for possible variations of the binding energy within the parameters regime where it was shown to be a good approximation.

[1] R. Rapaport and G. Chen, Experimental methods and analysis of cold and dense dipolar exciton fluids, J. Phys.: Condens. Matter **19**, 295207 (2007).

[2] L. V. Butov, Condensation and pattern formation in cold exciton gases in coupled quantum wells, J. Phys.: Condens. Matter **16**, R1577 (2004).

[3] L. V. Butov, Cold exciton gases in coupled quantum well structures, J. Phys.: Condens. Matter **19**, 295202 (2007).

[4] L. V. Butov, A. C. Gossard, and D. S. Chemla, Macroscopically ordered state in an exciton system, Nature (London) **418**, 751 (2002).

[5] D. Snoke, S. Denev, Y. Liu, L. Pfeiffer, and K. West, Long-range transport in excitonic dark states in coupled quantum wells, Nature (London) **418**, 754 (2002).

[6] R. Rapaport, G. Chen, D. Snoke, S. H. Simon, L. Pfeiffer, K. West, Y. Liu, and S. Denev, Charge Separation of Dense Two-Dimensional Electron-Hole Gases: Mechanism for Exciton Ring Pattern Formation, Phys. Rev. Lett. **92**, 117405 (2004).

[7] L. V. Butov, L. S. Levitov, A. V. Mintsev, B. D. Simons, A. C. Gossard, and D. S. Chemla, Formation Mechanism and Low-Temperature Instability of Exciton Rings, Phys. Rev. Lett. **92**, 117404 (2004).

[8] A. A. High, A. T. Hammack, J. R. Leonard, S. Yang, L. V. Butov, T. Ostatnicky, M. Vladimirova, A. V. Kavokin, T. C. H. Liew, K. L. Campman, and A. C. Gossard, Spin Currents in a Coherent Exciton Gas, Phys. Rev. Lett. **110**, 246403 (2013).

[9] B. Laikhtman and R. Rapaport, Exciton correlations in coupled quantum wells and their luminescence blue shift, Phys. Rev. B **80**, 195313 (2009).

[10] Y. Shilo, K. Cohen, B. Laikhtman, K. West, L. Pfeiffer, and R. Rapaport, Particle correlations and evidence for dark state condensation in a cold dipolar exciton fluid, Nat. Commun. **4**, 2335 (2013).

[11] G. J. Schinner, J. Repp, E. Schubert, A. K. Rai, D. Reuter, A. D. Wieck, A. O. Govorov, A. W. Holleitner, and J. P. Kotthaus, Confinement and Interaction of Single Indirect Excitons in a Voltage-Controlled Trap Formed Inside Double InGaAs Quantum Wells, Phys. Rev. Lett. **110**, 127403 (2013).

[12] K. Cohen, M. Khodas, B. Laikhtman, P. V. Santos, and R. Rapaport, Vertically coupled dipolar exciton molecules, Phys. Rev. B **93**, 235310 (2016).

[13] L. V. Butov, C. W. Lai, A. L. Ivanov, A. C. Gossard, and D. S. Chemla, Towards Bose-Einstein condensation of excitons in potential traps, Nature (London) **417**, 47 (2002).

[14] M. Combescot, O. Betbeder-Matibet, and R. Combescot, Bose-Einstein Condensation in Semiconductors: The Key Role of Dark Excitons, Phys. Rev. Lett. **99**, 176403 (2007).

[15] M. Alloing, M. Beian, M. Lewenstein, D. Fuster, Y. González, L. González, R. Combescot, M. Combescot, and F. Dubin, Evidence for a Bose-Einstein condensate of excitons, Europhys. Lett. **107**, 10012 (2014).

[16] M. Stern, V. Umansky, and I. Bar-Joseph, Exciton liquid in coupled quantum wells, Science **343**, 55 (2014).

[17] K. Cohen, Y. Shilo, K. West, L. Pfeiffer, and R. Rapaport, Dark high density dipolar liquid of excitons, Nano Lett. **16**, 3726 (2016).

[18] R. Rapaport, G. Chen, S. Simon, O. Mitrofanov, L. Pfeiffer, and P. M. Platzman, Electrostatic traps for dipolar excitons, Phys. Rev. B **72**, 075428 (2005).

[19] A. T. Hammack, M. Griswold, L. V. Butov, L. E. Smallwood, A. L. Ivanov, and A. C. Gossard, Trapping of Cold Excitons in Quantum Well Structures with Laser Light, Phys. Rev. Lett. **96**, 227402 (2006).

[20] K. Kowalik-Seidl, X. P. Vögele, B. N. Rimpfl, G. J. Schinner, D. Schuh, W. Wegscheider, A. W. Holleitner, and J. P. Kotthaus, Tunable photoemission from an excitonic antitrap, Nano Lett. **12**, 326 (2012).

[21] M. Alloing, A. Lemaître, E. Galopin, and F. Dubin, Optically programmable excitonic traps, Sci. Rep. **3**, 1578 (2013).

[22] A. A. High, E. E. Novitskaya, L. V. Butov, M. Hanson, and A. C. Gossard, Control of exciton fluxes in an excitonic integrated circuit, Science **321**, 229 (2008).

[23] A. Violante, K. Cohen, S. Lazic, R. Hey, R. Rapaport, and P. V. Santos, Dynamics of indirect exciton transport by moving acoustic fields, New J. Phys. **16**, 033035 (2014).

[24] A. G. Winbow, J. R. Leonard, M. Remeika, Y. Y. Kuznetsova, A. A. High, A. T. Hammack, L. V. Butov, J. Wilkes, A. A. Guenther, A. L. Ivanov, M. Hanson, and A. C. Gossard, Electrostatic Conveyer for Excitons, Phys. Rev. Lett. **106**, 196806 (2011).

[25] K. Cohen, R. Rapaport, and P. V. Santos, Remote Dipolar Interactions for Objective Density Calibration and Flow Control of Excitonic Fluids, Phys. Rev. Lett. **106**, 126402 (2011).

[26] S. Lazić, A. Violante, K. Cohen, R. Hey, R. Rapaport, and P. V. Santos, Scalable interconnections for remote indirect exciton systems based on acoustic transport, Phys. Rev. B **89**, 085313 (2014).

[27] J. R. Leonard, Y. Y. Kuznetsova, S. Yang, L. V. Butov, T. Ostatnický, A. Kavokin, and A. C. Gossard, Spin Transport of Excitons, Nano Lett. **9**, 4204 (2009).

[28] K. Kowalik-Seidl, X. P. Vögele, B. N. Rimpfl, S. Manus, J. P. Kotthaus, D. Schuh, W. Wegscheider, and A. W. Holleitner, Long exciton spin relaxation in coupled quantum wells, Appl. Phys. Lett. **97**, 011104 (2010).

[29] P. Rivera, J. R. Schaibley, A. M. Jones, J. S. Ross, S. Wu, G. Aivazian, P. Klement, K. Seyler, G. Clark, N. J. Ghimire, J. Yan, D. G. Mandrus, W. Yao, and X. Xu, Observation of long-lived interlayer excitons in monolayer $MoSe_2$-WSe_2 heterostructures, Nat. Commun. **6**, 6242 (2015).

[30] P. Rivera, K. L. Seyler, H. Yu, J. R. Schaibley, J. Yan, D. G. Mandrus, W. Yao, and X. Xu, Valley-polarized exciton dynamics in a 2d semiconductor heterostructure, Science **351**, 688 (2016).

[31] J. I. A. Li, T. Taniguchi, K. Watanabe, J. Hone, A. Levchenko, and C. R. Dean, Negative Coulomb Drag in Double Bilayer Graphene, Phys. Rev. Lett. **117**, 046802 (2016).

[32] J. I. A. Li, T. Taniguchi, K. Watanabe, J. Hone, and C. R. Dean, Excitonic superfluid phase in Double Bilayer Graphene, arXiv:1608.05846 (2016).

[33] P. Cristofolini, G. Christmann, S. I. Tsintzos, G. Deligeorgis, G. Konstantinidis, Z. Hatzopoulos, P. G. Savvidis, and J. J. Baumberg, Coupling Quantum Tunneling with Cavity Photons, Science **336**, 704 (2012).

[34] I. Rosenberg, Y. Mazuz-Harpaz, R. Rapaport, K. West, and L. Pfeiffer, Electrically controlled mutual interactions of flying waveguide dipolaritons, Phys. Rev. B **93**, 195151 (2016).

[35] J. Wilkes and E. A. Muljarov, Dipolar polaritons in microcavity-embedded coupled quantum wells in electric and magnetic fields, Phys. Rev. B **94**, 125310 (2016).

[36] V. Shahnazaryan, O. Kyriienko, and I. A. Shelykh, Adiabatic preparation of a cold exciton condensate, Phys. Rev. B **91**, 085302 (2015).

[37] C. C. Phillips, R. Eccleston, and S. R. Andrews, Theoretical and experimental picosecond photoluminescence studies of the quantum-confined Stark effect in a strongly coupled double-quantum-well structure, Phys. Rev. B **40**, 9760 (1989).

[38] J. E. Golub, K. Kash, J. P. Harbison, and L. T. Florez, Long-lived spatially indirect excitons in coupled GaAs/$Al_xGa_{1-x}As$ quantum wells, Phys. Rev. B **41**, 8564 (1990).

[39] A. Alexandrou, J. A. Kash, E. E. Mendez, M. Zachau, J. M. Hong, T. Fukuzawa, and Y. Hase, Electric-field effects on exciton lifetimes in symmetric coupled GaAs/Al 0.3 Ga 0.7 As double quantum wells, Phys. Rev. B **42**, 9225 (1990).

[40] S. Charbonneau, M. L. W. Thewalt, E. S. Koteles, and B. Elman, Transformation of spatially direct to spatially indirect excitons in coupled double quantum wells, Phys. Rev. B **38**, 6287 (1988).

[41] I. Galbraith and G. Duggan, Exciton binding energy and external-field-induced blue shift in double quantum wells, Phys. Rev. B **40**, 5515 (1989).

[42] T. Kamizato and M. Matsuura, Excitons in double quantum wells, Phys. Rev. B **40**, 8378 (1989).

[43] J. Lee, M. O. Vassell, E. S. Koteles, and B. Elman, Excitonic spectra of asymmetric, coupled double quantum wells in electric fields, Phys. Rev. B **39**, 10133 (1989).

[44] M. M. Dignam and J. E. Sipe, Exciton states in coupled double quantum wells in a static electric field, Phys. Rev. B **43**, 4084 (1991).

[45] I. Linnerud and K. A. Chao, Exciton binding energies and oscillator strengths in a symmetric $Al_xGa_{1-x}As$/GaAs double quantum well, Phys. Rev. B **49**, 8487 (1994).

[46] Y. Takahashi, Y. Kato, S. S. Kano, S. Fukatsu, Y. Shiraki, and R. Ito, The effect of electric field on the excitonic states in coupled quantum well structures, J. Appl. Phys. **76**, 2299 (1994).

[47] J. Soubusta, R. Grill, P. Hlidek, M. Zvara, L. Smrcka, S. Malzer, W. Geisselbrecht, and G. H. Dohler, Excitonic photoluminescence in symmetric coupled double quantum wells subject to an external electric field, Phys. Rev. B **60**, 7740 (1999).

[48] M. H. Szymanska and P. B. Littlewood, Excitonic binding in coupled quantum wells, Phys. Rev. B **67**, 193305 (2003).

[49] S. C. Arapan and M. A. Liberman, Exciton levels and optical absorption in coupled double quantum well structures, J. Lumin. **112**, 216 (2005).

[50] K. Sivalertporn, L. Mouchliadis, A. L. Ivanov, R. Philp, and E. A. Muljarov, Direct and indirect excitons in semiconductor coupled quantum wells in an applied electric field, Phys. Rev. B **85**, 045207 (2012).

[51] D. S. Citrin, Radiative lifetimes of excitons in quantum wells: Localization and phase-coherence effects, Phys. Rev. B **47**, 3832 (1993).

[52] K. Sivalertporn, Effect of barrier width on the exciton states in coupled quantum wells in an applied electric field, Phys. Lett. A **380**, 1990 (2016).

[53] G. Bastard, *Wave Mechanics Applied to Semiconductor Heterostructures*, Monographies de physique (Halsted, New York, 1988).

[54] P. Harrison, *Quantum Wells, Wires, and Dots: Theoretical and Computational Physics* (Wiley, New York, 2000).